

Calculations of near-field emissions in frequency-domain into time-dependent data with arbitrary wave form transient perturbations

Yang Liu¹, Blaise Ravelo¹ and Jalel Ben Hadj Slama²

¹IRSEEM (Institut de Recherche en Systèmes Electroniques Embarqués), EA 4353,

At the graduate school of engineering ESIGELEC,
Av. Galilée, BP 10024, 76801 Saint Etienne du Rouvray, France.

²National Engineering School of Sousse, (ENISo),
Technopole de Sousse, 4054 Sousse, Tunisia.

Tel.: +33 (0)2 32 91 59 71

Fax: +33 (0)2 32 91 58 59

E-mail: yang.liu@esigelec.fr, blaise.ravelo@esigelec.fr, bhslama@yahoo.fr

Abstract

This paper is devoted on the application of a computational method for calculating transient electromagnetic (EM) near-field (NF) radiated by electronic structures excited by arbitrary wave form perturbations $i(t)$ from frequency-dependent data. The method proposed is based on the applications of fast Fourier transform (FFT). The steps illustrating the proposed method principle are described. It is based on three successive steps: the synchronization of the input excitation spectrum $I(f)$ and the given frequency NF data $H_0(f)$, the convolution of inputs data and then, the determination of the time-domain NF emissions $H(t)$. The method feasibility is verified by simulations from EM 3D standard tools. In addition, a time-frequency extraction technique of the time-dependent z-transversal NF component $X_z(t)$ from the frequency-dependent longitudinal components $X_x(f)$ and $X_y(f)$ is also presented. This technique is based on the conjugation of the plane wave spectrum (PWS) transform and FFT. Verification with NF radiated by a set of dipole radiations is made. The method introduced in this paper is particularly useful for investigating time-domain emissions for EMC applications by considering transient EM interferences (EMIs).

Keywords: Near-field (NF) emission, transient perturbations, electromagnetic compatibility (EMC), FFT, plane wave spectrum (PWS), time-frequency method, time-domain computational method.

1. Introduction

With the unintentional electromagnetic interferences (EMIs), the design engineers need to take into account the electromagnetic compatibility (EMC) models during the electronic systems manufacture process [1-3]. The most disturbing EMC effects caused by the electrical/electronic system integration can be due to the EM near-field (NF) radiations and the couplings between the different circuits

as the electrical cables and electronic equipments [4-5]. Therefore, NF emission models and scanning measurement techniques were proposed [6-9]. Nevertheless, large amount of the NF investigation were performed in frequency-domain. However, the transient perturbations are susceptible to degrade the mixed electronic systems as digital and radio frequencies (RFs) [10] and integrated systems [11]. It has been found that the EMC engineering should include the transient EM-NF emissions especially in time-domain [10-20]. Currently, this topic attracts many of electronic engineers and researchers. With the increase of integration density and the operating rate, EM NF analysis is necessary for the RF/digital electronic boards [1-3]. Undesired transient effects can be created by different perturbations as the non-linearity of electronic devices during their commutations [10]. These transient EM-field emissions need to be canceled out for the reliability. For this reason, EM transient analysis is required. As reported in [21], analog/mixed (AM) electronic designers use regularly software tools such as SPICE, while those working on RF/microwave engineering focus in frequency-domain simulation tools based on the S-parameters. In practice, one needs the fusion of both approaches as AM engineers are required to make further analysis on the critical components by using EM simulation tools. This constitutes an improvement technique in the EMC area. In this optic, the EM emission modeling by the mixed components becomes one of the crucial steps before the implementation. Therefore, the issues both in frequency- and time-domains should be forecasted.

Basically, the transient EM-field computation was initially determined with elementary EM dipole radiations [22-27]. As reported in [7-8], any electronic circuit NF radiations can be reproduced with arrays of elementary dipoles. Moreover, time-domain NF radiation was also conducted with excitation based on the arbitrary wave form signals [28]. This computational approach is advantageous for the modeling of EMNF radiated by complex electrical/electronic structures which cannot be modeled with most of standard tools [29-30]. This computation

method remains complicated when considering electronic devices operating with UWB and base band signal. So, more recently, EM computational method based on the plane wave spectrum (PWS) theory was proposed [31-33]. This method is based on the exploitation of the fundamental plane wave's properties and FFT, then, transposed in time-domain. It allows simplifying considerably the reconstruction of the EM NF radiations (including the evanescent waves) as the calculation of longitudinal component (along z -axis) from transversal components (along x - and y -axes) [31-32], the NF/NF transform [33] and also extraction of the electric NF components (E_x , E_y and E_z) from 2D data H_x and H_y [34]. In the continuation of these works, as a special issue of [35], the generalized methodology of a time-frequency EM NF computation is presented in this paper.

The paper is mainly divided in three sections. Section 2 is focused on the application of the routine algorithm of EM NF time-frequency method proposed in [28][35]. Section 3 introduces a time-domain EM computation method based on the PWS transform for extracting EM NF component X_z from X_x and X_y with arbitrary excitations. Section 4 is the conclusion.

2. Calculation method of time-dependent near-field maps with transient perturbations from frequency-dependent data

This section describes the time-frequency computation methodology presented in this. The basic theoretical approach and the routine algorithm are detailed. In this paper, we will extend the FFT and IFFT instructions to reconstitute the time-dependent magnetic NF maps $H_{x,y,z}(t)$ radiated by an electronic device from the frequency components $H_{x,y,z}(f)$ for any excitation undesired currents or voltages for the EMC applications as proposed in [28][35].

2.1. Theoretical approach of the time-frequency computation method under study

Let us consider the time-dependent plot of the arbitrary signal $x(t)$ presented in Figure 1. This signal is supposed as the excitation of the electronic structure under consideration. As indicated in this figure, the sampled data corresponding to the signal under test is supposed and discretized from the starting time t_{min} to the stop time t_{max} with time step Δt . It means that the number of time-dependent samples is equal to:

$$n = \text{int}\left(\frac{t_{max} - t_{min}}{\Delta t}\right), \quad (1)$$

with $\text{int}(\alpha)$ generates the lowest integer number greater than the real number α .

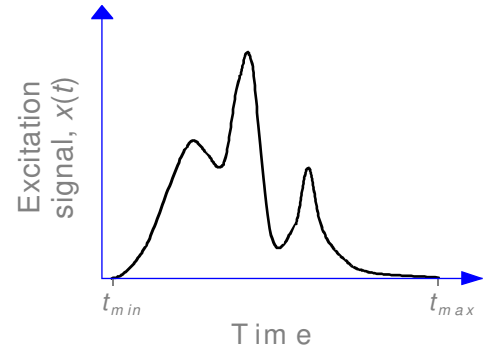


Figure 1: Transient excitation signal.

By definition, we can determine mathematically the frequency-dependent spectrum of $i(t)$ as a complex number denoted as:

$$\underline{I}(f_k) = \text{fft}[i(t_k)], \quad (2)$$

where $t_k = k \cdot \Delta t$ and $k = \{1 \dots n\}$. In this expression, the variable f_k represents the sampling of the frequency variable. These frequencies can be extracted from the sampling time parameters by the following expression:

$$f_k = k \cdot \Delta f, \quad (3)$$

with $k = \{1 \dots n\}$ and Δf is the step frequency which is determined by the relation:

$$\Delta f = \frac{1}{t_{max} - t_{min}}. \quad (4)$$

In order to operate with the excitation signal, the frequency spectrum magnitude needs to be normalized as a complex coefficient. For this reason, \underline{I}_0 is assumed as a harmonic component sinusoidal current necessary for generating the electric or magnetic field spectrum $\underline{H}_0(f)$, the harmonics of the input current can be normalized with the following complex coefficients:

$$\underline{c}_k = \frac{\underline{I}(f_k)}{\underline{I}_0}, \quad (5)$$

This normalization is illustrated by spectrum representation shown in Figure 2 [27].

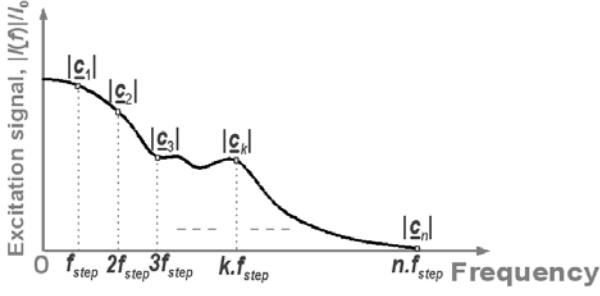


Figure 2: Extraction of the frequency spectrum coefficients from the excitation signal spectrum.

For the base band applications, it is interesting to note that the starting frequency f_{min} must be equal to the frequency step Δf . In this scope, the spectrum value can be extrapolated linearly to generate the DC-component of the excitation signal. According to the signal processing theory, the DC-component of the ultra-short transient signal is negligible at very low frequency band. So, the extrapolation operating will not change the calculation results. The upper frequency f_{max} must belong in the frequency bandwidth containing higher than 95% spectrum energy of the excitation signal.

Once, the frequency spectrum coefficients are defined, the time-dependent NF data corresponding to the transient current signal can be carried out by convoluting the frequency coefficients c_k and the frequency-domain field data. The routine process will be presented in the next subsection.

2.2. Computational process of the proposed method

The computation method developed in this paper can be summarized in two steps. After extracting the frequency spectrum coefficient c_k from the transient excitation signal $i(t)$ as explained in the previous subsection, we will focus on the convolution between frequency spectrum coefficients and the frequency EM field data.

Let us denote $\underline{H}(x, y, z_0, f)$ the frequency dependent magnetic field recorded in the plane $z = z_0$ above the considered radiating electronic device as highlighted by Figure 3.

The frequency EM field data $\underline{H}(x, y, z_0, f)$ can be obtained by 2D measurements or simulations with standard commercial tools.

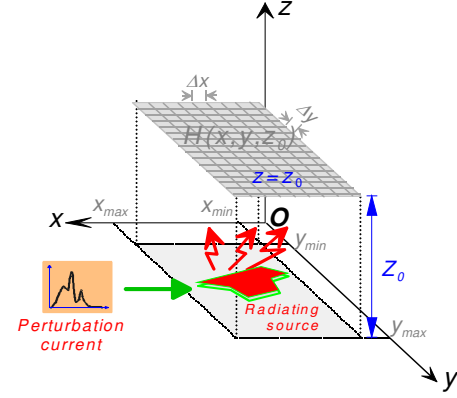


Figure 3: Representation of the magnetic NF scanned in the plane placed at the height z_0 above the radiating device.

In this case, we emphasize that the frequency EM field data $\underline{H}(x, y, z_0, f)$ needs to be synchronized with the specific frequency interval $[f_{min}, f_{max}]$ of the transient excitation signal $i(t)$ and the frequency step Δf . As presented in Figure 3, the magnetic NF time-dependent data $\underline{H}(x, y, z_0, t)$ is generated by the device under test excited by the current $i(t)$. As argued above, the magnetic NF data $\underline{H}(x, y, z_0, t)$ can be determined with the IFFT by the convolution product of the frequency coefficient c_k and the frequency dependent NF data $\underline{H}(x, y, z_0, f)$ via the following equation:

$$\underline{H}(x, y, z_0, t) = \text{ifft}[c_k \cdot \underline{H}(x, y, z_0, f)], \quad (6)$$

To reconstitute the time-domain results, the imaginary part of the data $\underline{H}(x, y, z_0, t)$ is not necessary. Therefore, the desired time-domain results are obtained with the expression:

$$H(x, y, z_0, t) = \text{Real}[\underline{H}(x, y, z_0, t)], \quad (7)$$

where the function $\text{Real}(\alpha)$ represents the real part of the complex number α . The routine process of the proposed computation method is presented in Figure 4 [35]. This workflow is performed with different operations in order to provide the time-domain EM NF radiated by the device under test with the arbitrary transient excitation signal $i(t)$.

To validate the investigated method, a Matlab program has been implemented according to the routine algorithm described in Figure 4.

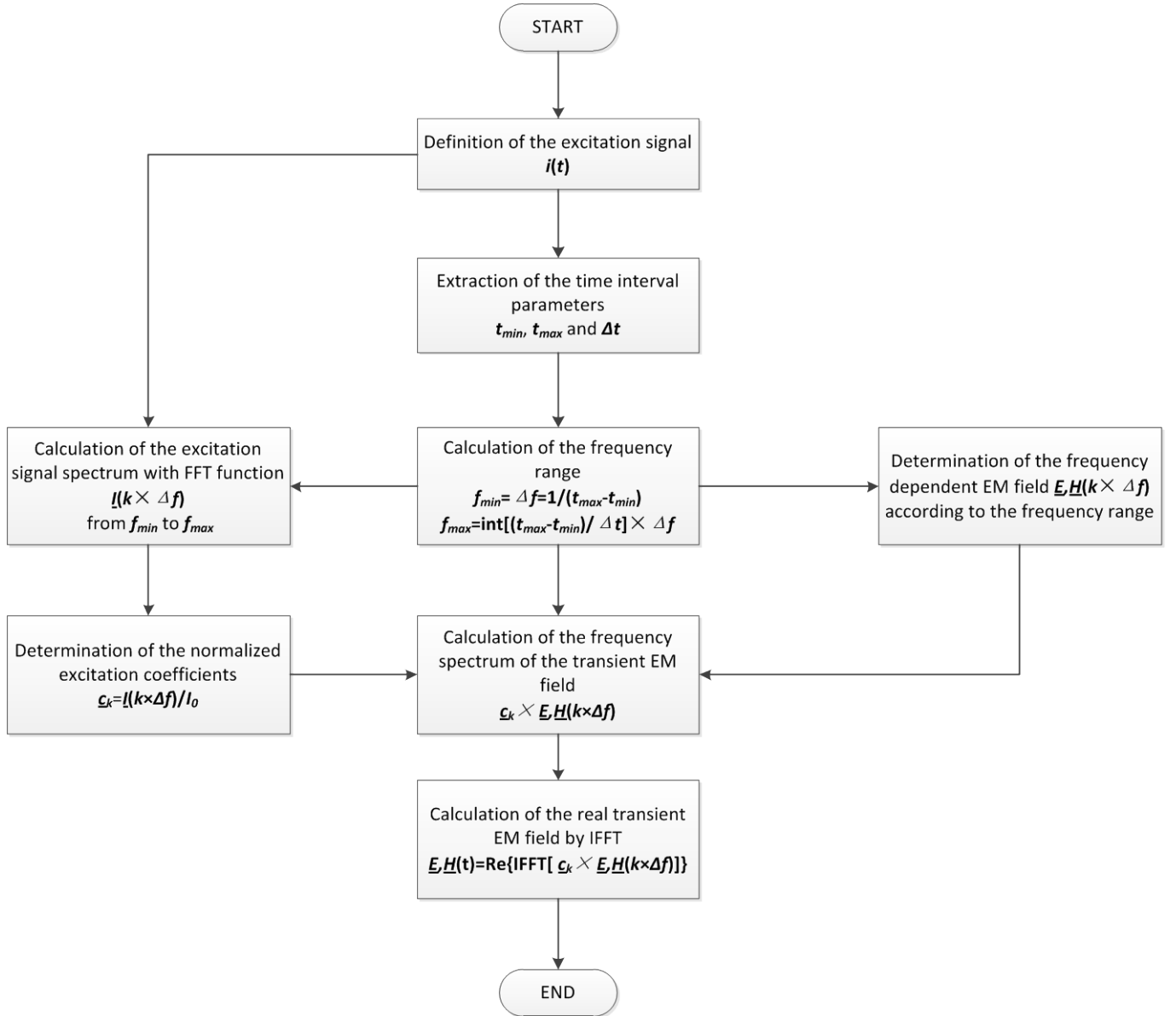


Figure 4: Routine process of the time-frequency computation method proposed [35].

2.3. Illustration results

In this subsection, a comparison between the transient EM-field radiated by a concrete microstrip device described from the 3 D s oftware s imulation and those obtained from the proposed method is realized.

2.3.1. Description of the Assumed Excitation Signal

In order to highlight the influence of the form and the transient variation of the disturbing currents in the electronic structure, the considered short-duration pulse excitation current $i(t)$ is assumed as a Gaussian signal modulating 1.25 GHz sine carrier, defined by the analytical formula:

$$i(t) = I_M \cdot \exp\left(-\frac{(t-t_0)^2}{2\Delta t^2}\right) \cdot \sin(2\pi f_0 t), \quad (8)$$

Figure 5 displays respectively, the transient plot of this signal and its frequency spectrum. In practice, the time interval range is defined from $t_{min} = 0$ ns to $t_{max} = 14.218$ ns with step $\Delta t = 0.1436$ ns.

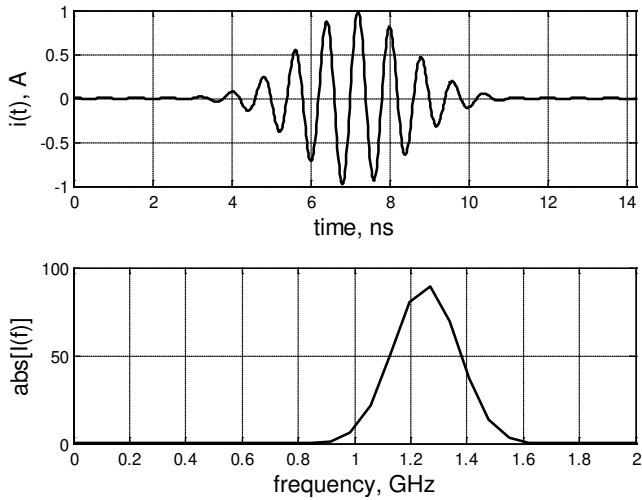


Figure 5: Transient plot of the considered excitation current $i(t)$ and its frequency spectrum $I(f)$.

One can see that this modulated signal presents a frequency bandwidth of 0.5 GHz, where belongs more than 95-% of the spectrum signal energy. The calculated data $\underline{I}(f) = \mathcal{F}\{i(t)\}$ implies the frequency coefficient values of $i(t)$ according to the definition expressed in (8) as described earlier in subsection 2.2.

2.3.2 Description of the device under test

The microstrip circular resonator shown in Figure 6 was designed and considered as the device under test in order to validate the method under investigation. The resonator is based on a substrate with relative permittivity $\epsilon = 10$. It is fed by the via hole port with the transient current presented above. The top view of the resonator is shown by Figure 6.

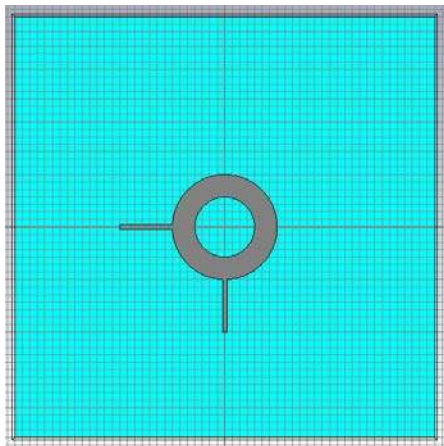


Figure 6: Top view of the microstrip circular resonator.

To validate the method proposed in this paper, comparisons of different results were made between the CST Microwave simulations and the computation method proposed.

2.3.3. Transient EM-Field Determined by CST MWS simulation

By considering the circular resonator presented in Figure 6, excited by the pulse current plotted in Figure 5 yields the electric and magnetic field components mappings depicted in Figure 7 and Figure 8 at the arbitrary time $t_0 = 7.611$ ns and in the horizontal plan parallel to (Oxy) referenced by $z_0 = 2$ mm. The dimensions of the mappings were set at $L_x = 56$ mm and $L_y = 56$ mm with resolutions respectively, equal to $\Delta x = 1$ mm and $\Delta y = 1$ mm.

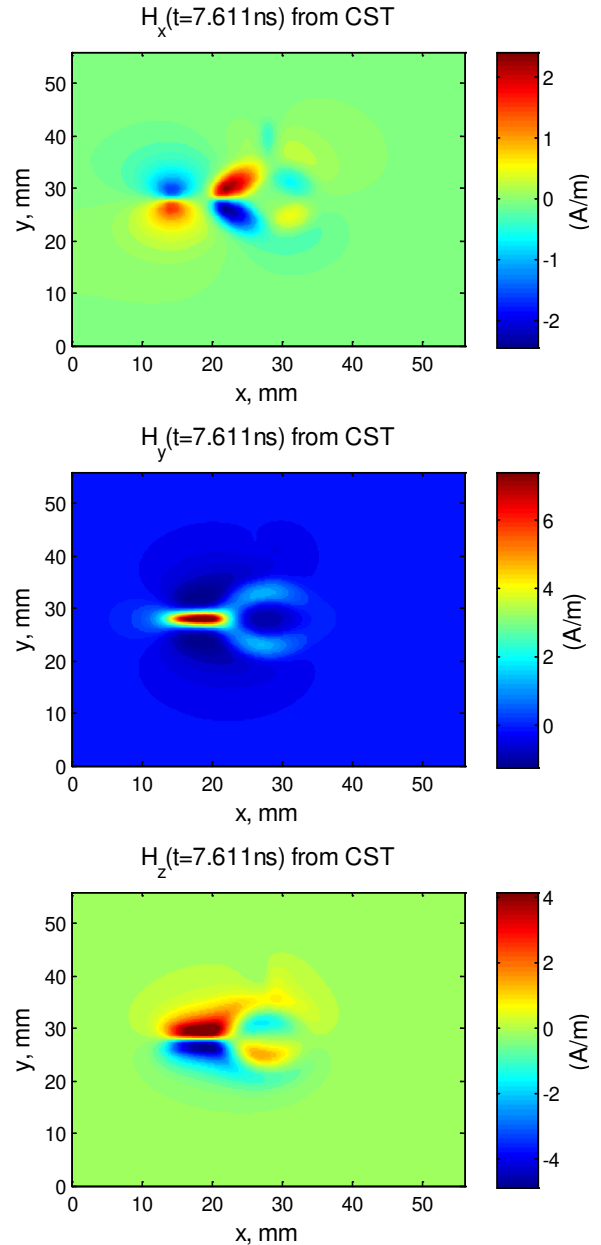


Figure 7: Cartographies of magnetic field components at $t=7.611$ ns obtained from the CST simulation.

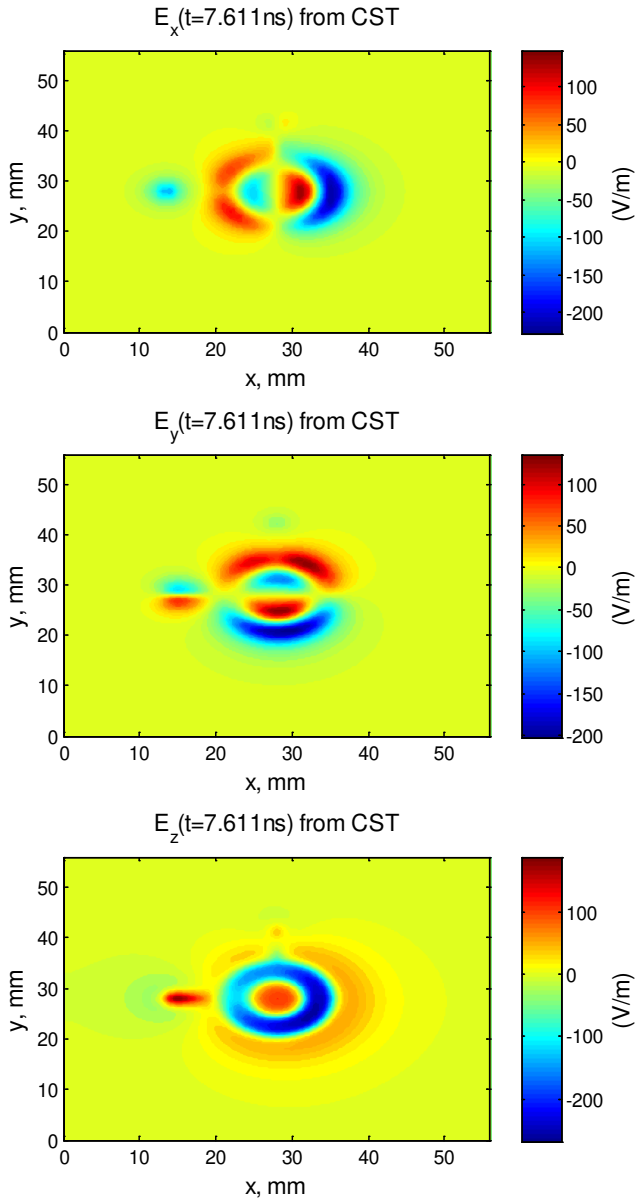


Figure 8 : Cartographies of the electric field components at $t=7.611\text{ ns}$ obtained from the CST simulation.

2.3.4. Computed Results from the Proposed Method

First, by analyzing the frequency-domain results achieved by CST Microwave Studio, one obtains the cartographies of the frequency-dependent electric and magnetic field from $f_{min} = 1\text{ GHz}$ to $f_{max} = 1.5\text{ GHz}$ step $\Delta f = 0.01\text{ GHz}$.

After the program execution of the algorithm indicated by the flow chart described by Figure 4, one gets the results shown in Figure 9 and Figure 10 via the combination of the frequency-dependent data of the electric or magnetic field components associated to the frequency coefficient of the excitation signal. One can see that one establishes the cartographies having the same behaviors as those generated via the direct calculations

displayed in Figure 7 and Figure 8.

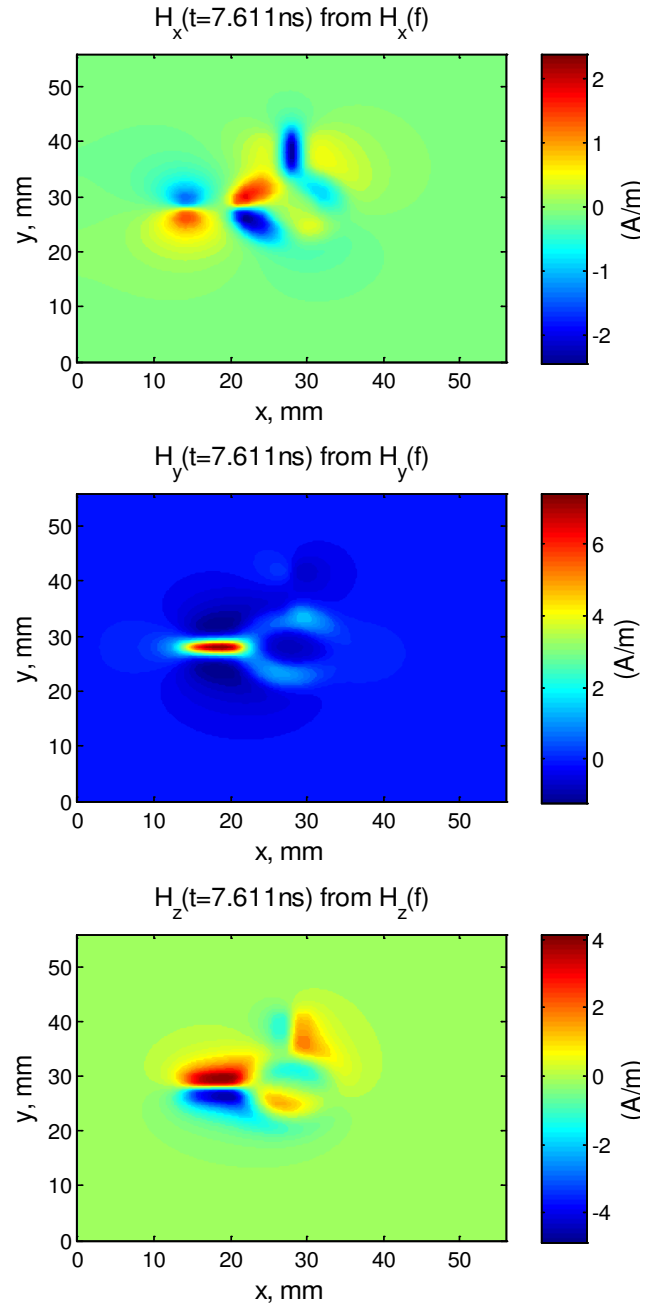


Figure 9: Cartographies of magnetic field components: obtained from the proposed time-frequency computation method.

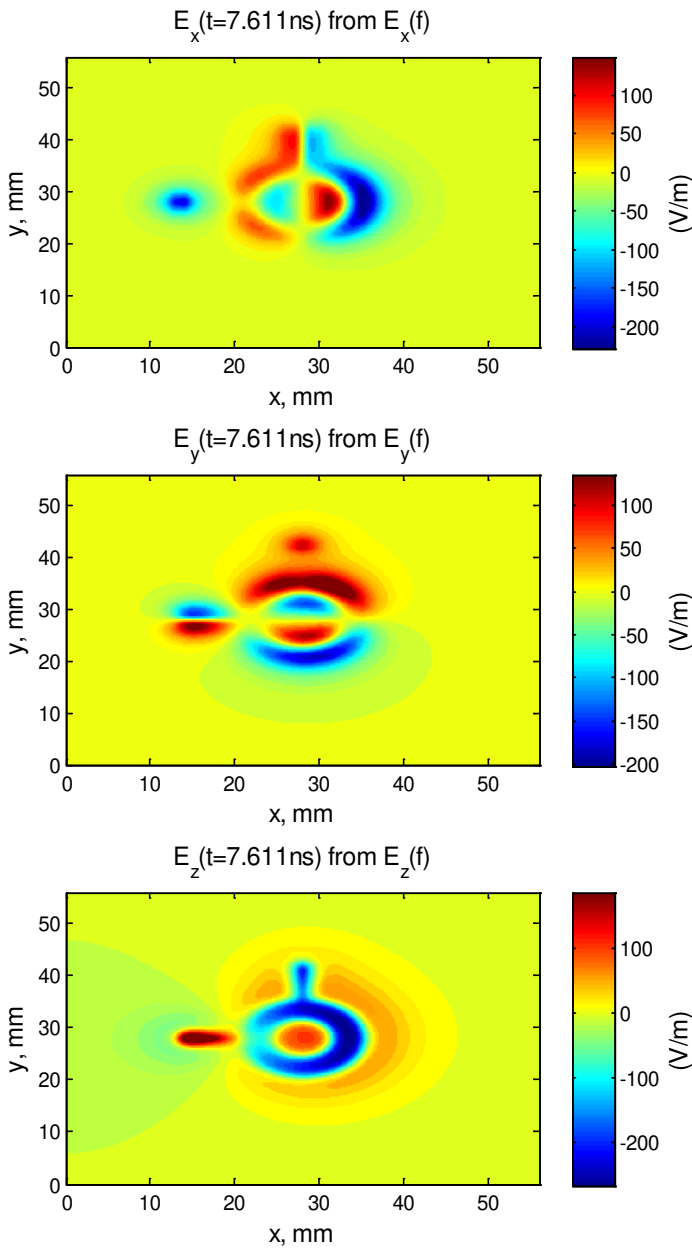


Figure 10: Cartographies of electric field components: obtained from the proposed time-frequency computation method.

Furthermore, as illustrated by Figure 11 and Figure 12, a very good correlation between the profiles along Ox or Oy of the EM field components detected in the vertical plane placed at $x = 22\text{ mm}$ or $y = 30.3\text{ mm}$ was observed.

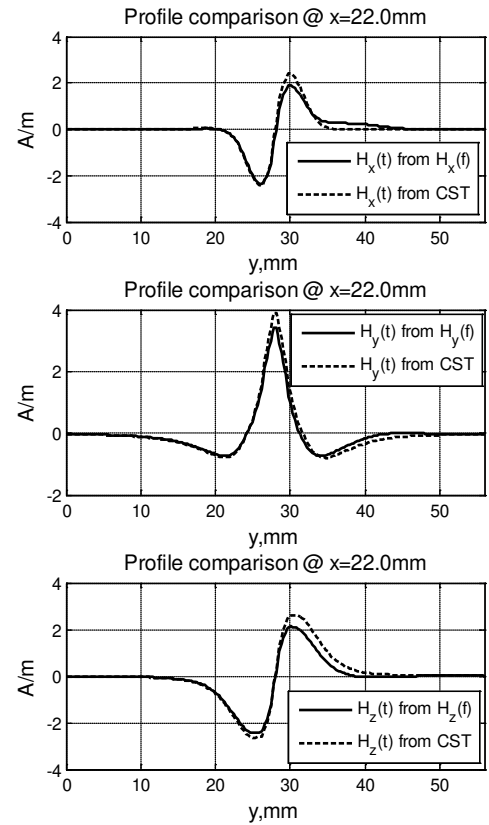


Figure 11: Comparisons of the magnetic field components profiles obtained from the proposed time-frequency computation method and the direct calculation, detected in the vertical plane $x = 22\text{ mm}$.

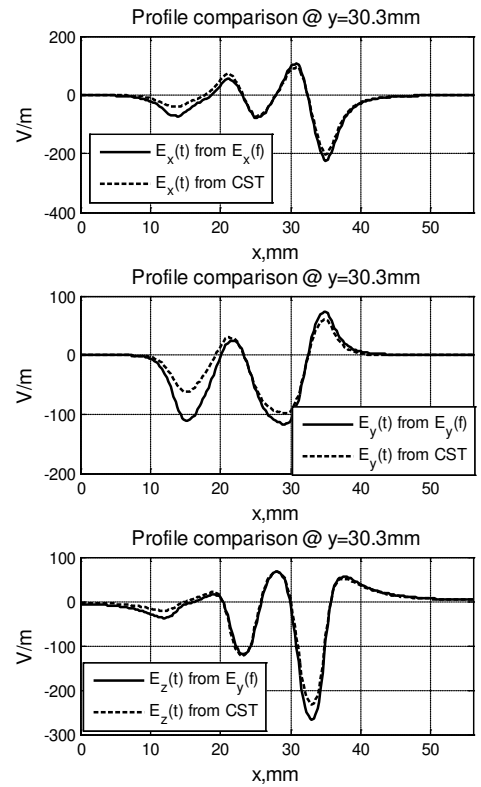


Figure 12: Comparisons of the electric field components profiles obtained from the proposed time-frequency computation method and the direct calculation, detected in the vertical plane placed at $y=30.3\text{mm}$.

In addition to this computation method, we propose further method enabling to extract the third component (along z -direction) of EM fields in time-domain knowing the two first components (along x - and y -directions) in the next section.

3. Extraction method of the transverse component $X_z(t)$ from $X_x(f)$ and $X_y(f)$ with ultra-short duration transient perturbations

To reduce the order of complexity and the processing time of measurement, we propose a method to extract the time EM transversal component $X_z(t)$ from the known the longitudinal components $X_x(t)$ and $X_y(t)$. To do this, we use the Plane Wave Spectrum (PWS) method associated with the radiation of electric dipoles in the time domain as introduced recently in [31-32].

The basic approach of EM field characterization in time domain is extracted from the frequency data combined via FFT. First, the PWS theory which was initially introduced in [36-38] will be applied to the obtained data in frequency domain. Finally, the frequency data will be transposed in to time domain with IFFT.

3.1. Principle of the time-frequency method of the z -component calculation from x -/ y -components of the EM NF

By definition, the PWS method [31-33][36-38] is a basic method dedicated to the decomposition of any EM-field plotted in 2D as a sum of plane waves propagating in different space directions. One denotes:

$$\vec{k} = k_x \vec{u}_x + k_y \vec{u}_y + k_z \vec{u}_z, \quad (9)$$

the wave vector in the rectangular coordinate system ($Oxyz$) with unit vectors, \vec{u}_x , \vec{u}_y and \vec{u}_z . The modulus of this wave vector, what is also known as the wave number, is given by:

$$k(f) = \sqrt{k_x^2(f) + k_y^2(f) + k_z^2(f)} = \frac{2\pi}{\lambda(f)} = \frac{2\pi f}{v}. \quad (10)$$

where $\lambda(f)$ is the wavelength at the operating frequency f .

According to the PWS theory, the EM field $\vec{X}(x, y, z)$ can be expressed as a double integral of their PWS components $\vec{P}_X(k_x, k_y, z)$ with the following formulation:

$$\vec{X}(x, y, z) = \frac{1}{4\pi^2} \int_{-\infty}^{\infty} \int_{-\infty}^{\infty} \vec{P}_X(k_x, k_y, z) e^{j(k_x x + k_y y)} dk_x dk_y. \quad (11)$$

Similar to the 2D Fourier transform, the inverse PWS (IPWS) of EM field is given by the following equation:

$$\vec{P}_X(k_x, k_y, z) = \int_{-\infty}^{\infty} \int_{-\infty}^{\infty} [\vec{X}(x, y, z)] e^{-j(k_x x + k_y y)} dx dy, \quad (12)$$

The horizontal X - Y plane is with dimensions $L_x \times L_y$. It is discretized with the steps Δx and Δy , respectively, so that the discrete indexes, n_x and n_y , are:

$$k_x = \frac{2\pi}{x} = \frac{2\pi}{n_x \Delta x}, \quad (13)$$

$$k_y = \frac{2\pi}{y} = \frac{2\pi}{n_y \Delta y}. \quad (14)$$

In this case, the horizontal components of the wave vector k_x and k_y vary respectively between:

$$k_{x \min} = -\frac{\pi}{\Delta x}, \quad (15)$$

$$k_{y \min} = -\frac{\pi}{\Delta y}, \quad (16)$$

and

$$k_{x \max} = \frac{\pi}{\Delta x}, \quad (17)$$

$$k_{y \max} = \frac{\pi}{\Delta y}, \quad (18)$$

with the numerical step:

$$\Delta k_x = \frac{2\pi}{L_x}, \quad (19)$$

$$\Delta k_y = \frac{2\pi}{L_y}. \quad (20)$$

From equation (10), one can determine the corresponding vertical component [31-33][36-38]:

$$k_z = \begin{cases} \sqrt{k^2 - k_x^2 - k_y^2} & \text{if } k_x^2 + k_y^2 < k^2 \\ -j\sqrt{k_x^2 + k_y^2 - k^2} & \text{if } k_x^2 + k_y^2 > k^2 \end{cases}. \quad (21)$$

To avoid the unexpected case, the following relation must be respected.

$$\max(\Delta k_x, \Delta k_y) < \frac{2\pi}{\lambda}. \quad (22)$$

And also, at the boundary condition, the field components and their PWS components, $X_{x,y,z}$ and $P_{X_{x,y,z}}$ must tend to zero.

According to the plane wave properties, wave vectors \vec{k} and \vec{P} must be perpendicular to each other:

$$\vec{k} \cdot \vec{P} = 0 \Rightarrow k_x P_{X_x} + k_y P_{X_y} + k_z P_{X_z} = 0. \quad (23)$$

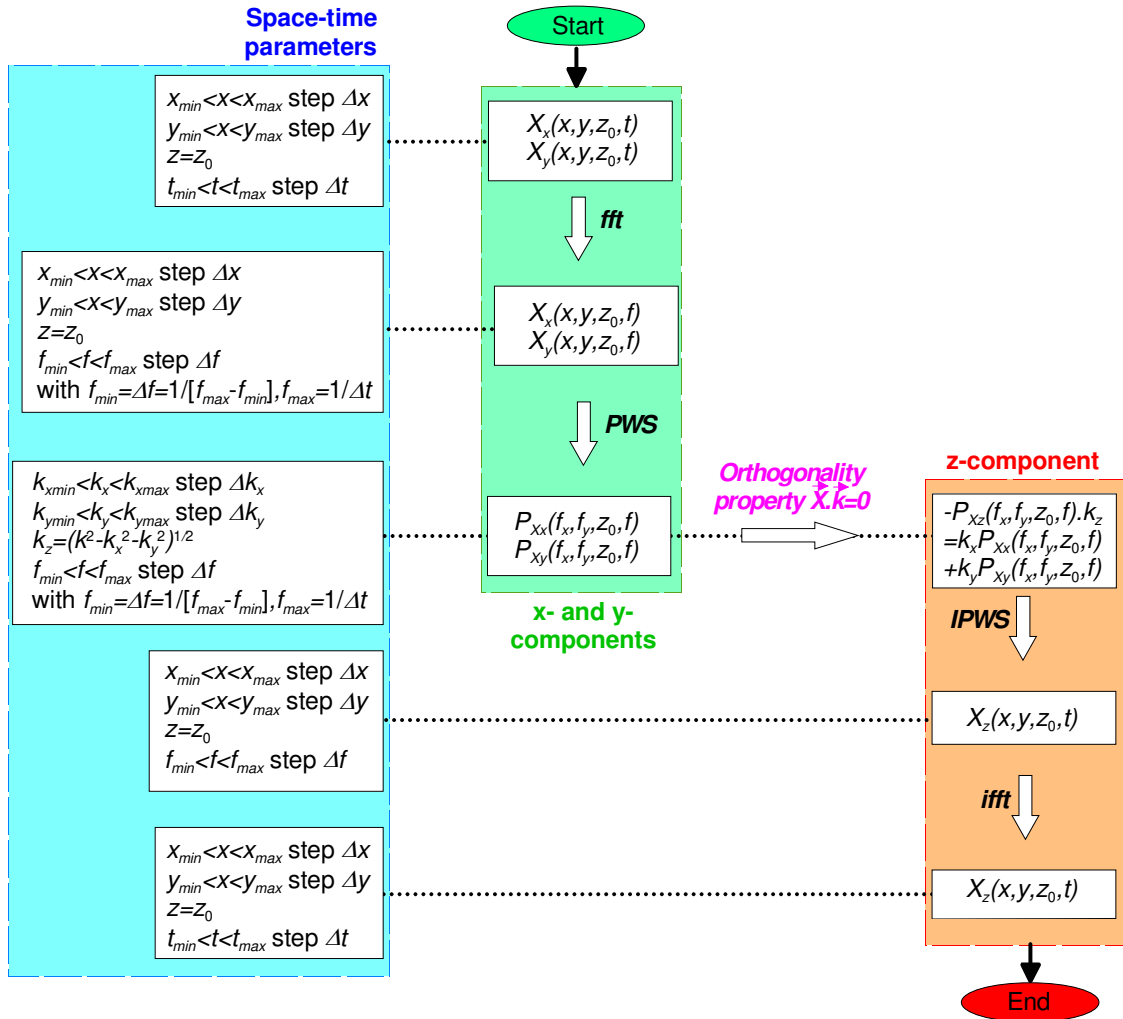


Figure 13: Routine algorithm illustrating the computation method of X_z from X_x and X_y by using the PWS transform.

So that, the vertical component P_{X_z} can be determined by the following equation:

$$P_{X_z} = -\frac{k_x P_{X_x} + k_y P_{X_y}}{k_z}. \quad (24)$$

All the approaches and calculations presented above work in the frequency domain. So, we need to transform the time domain data $X_x(t)$ and $X_y(t)$ into frequency domain by using the Fourier transform $X_{x,y}(f) = \text{fft}[X_{x,y}(t)]$. Also, at the end of this procedure, the z-component $X_z(f)$ must be transformed back into time domain by the inverse Fourier transform $X_z(t) = \text{ifft}[X_z(f)]$. Figure 11 summarizes the routine algorithm of the method proposed.

As a conclusion, all the procedure above means that P_{X_z} , obviously X_z , can be extracted from P_{X_x} and P_{X_y} which can be calculated from the IPWS equation expressed in (12) if the 2D data X_x and X_y are given. In summary, with the proposed method, the EM NF measurement processes can be simplified.

3.2. Application results

To validate the computation method proposed in this paper, a set of elementary electric dipoles with arbitrarily chosen configuration is placed in the X-Y plane as displayed in Figure 14. It is considered as a radiating source defined by analytical equations proposed in [39-41]. All the electric dipoles are simultaneously excited by the same time varying current $I(t)$. Figure 15 displays the current excitation. The frequency spectrum of $I(t)$ plotted in Figure 16 presents a maximum frequency of about 5 GHz.

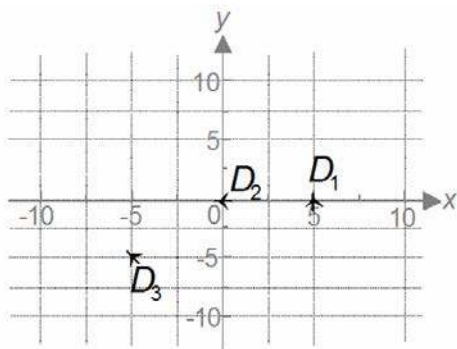


Figure 14: Assumed configuration of the set of three electric dipoles.

So, the minimum wavelength is $\lambda_{min} = c/f_{max} = 0.6$ m. According to the wave propagation theory, the NF zone is up to about $\lambda_{min}/10 = 6$ cm above the dipoles plane.

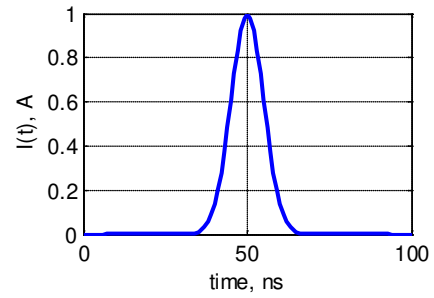


Figure 15: Time variation of the excitation signal.

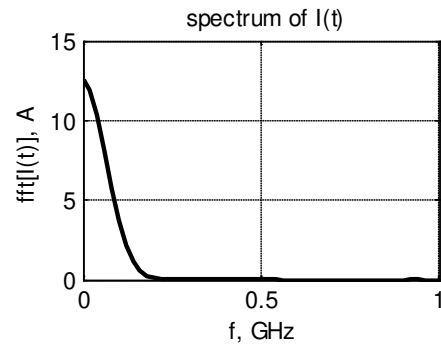


Figure 16: Frequency spectrum of the excitation signal $I(t)$ shown in Figure 15.

First, we will calculate the transient electric fields with formulae expressed in [39-40]. The results are shown in Figure 17, the plots plane is at the height $z = 10$ mm and at the time $t_0 = 50$ ns. The profile of the Electric field along the line equated by $x = 0$ mm is shown by Figure 18. The three transient electric field components are obtained at the three different point in the plane $z = 10$ mm, shown as Figure 19.

Second, the vertical electric field component $E_z(t)$ extracted by the PWS method will be compared with the own $E_z(t)$ calculated directly. This comparison is shown by Figure 19. The comparison of the E_z distribution at $t = 50$ ns across the horizontal plane at $z = 10$ mm, is shown in Figure 20. One can see a good agreement in the zone with higher field strengths with almost the same distribution.

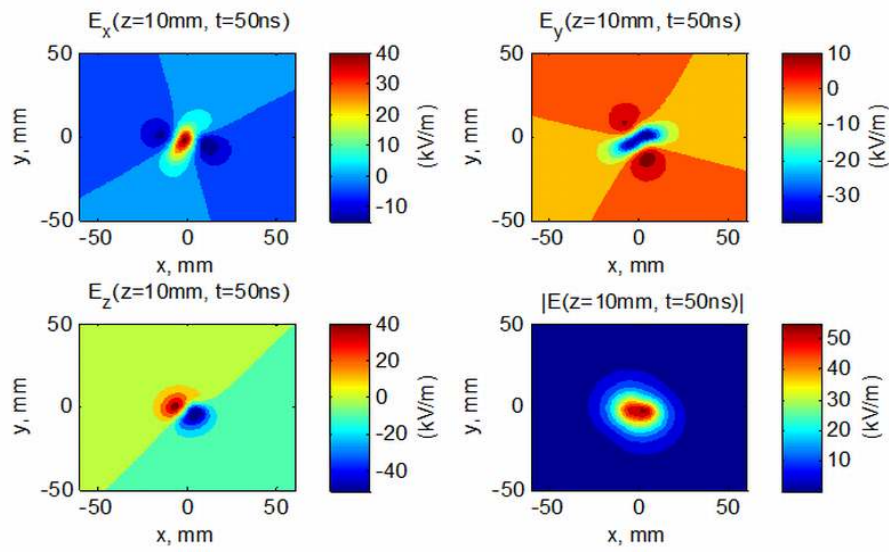


Figure 17: Calculated electric field components E_x , E_y and E_z and the total magnitude $|E|$ for the dipoles in Figure 14 at the horizontal plane at the height $z = 10$ mm at the instant time $t = 50$ ns.

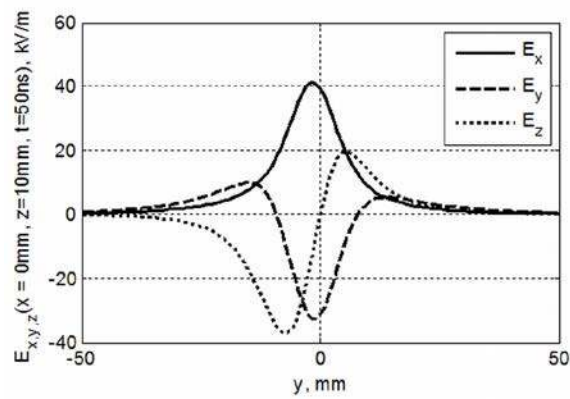


Figure 18: Calculated electric field components E_x , E_y and E_z for the dipoles in Figure 14 along the line $z = 10$ mm, $x = 0$ and at the instant time $t = 50$ ns.

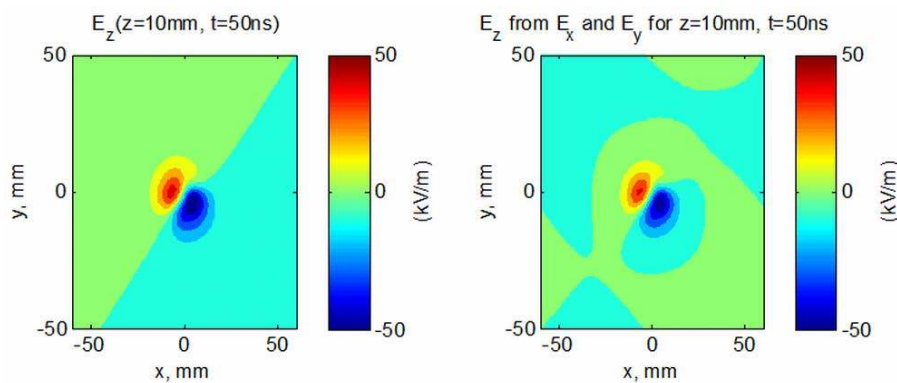


Figure 19: Comparison between the E_z components directly computed and extracted at the instant time $t = 50$ ns across the horizontal plane at $z = 10$ mm.

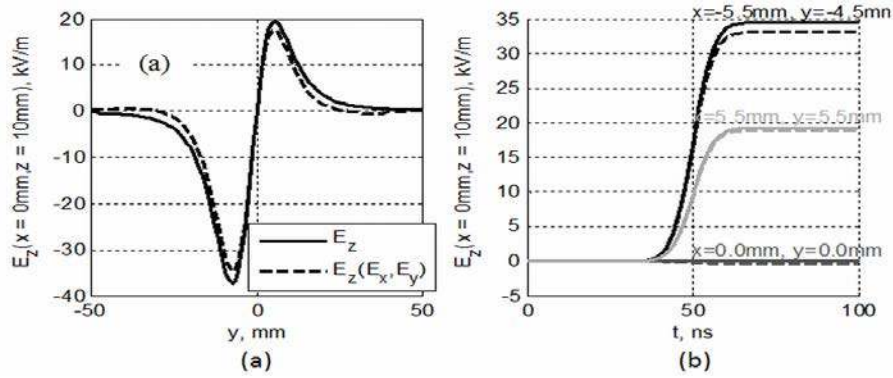


Figure 20: Comparison between directly computed and extracted E_z field: (a) at the instant time $t = 50$ ns along the line $z = 10$ mm, $x = 0$; (b) as a function of time at the points $(x,y) = \{(0,0), (-5.5\text{mm}, -4.5\text{mm}), (5.5\text{mm}, 4.5\text{mm})\}$ on the horizontal plane at $z = 10$ mm.

We can also find some errors in the zone with lower field strengths. However, these errors are relatively small. They can be visualised in Figure 20. We can see that the relative errors are very small at the randomly chosen points.

In order to verify the relevance of the proposed method, we also simulate the transient radiation of the set of dipoles in Figure 14 with commercial 3D EM modelling software, CST Microwave Studio™. Figure 21 describes the setup of the electric dipoles in CST MWS simulation.

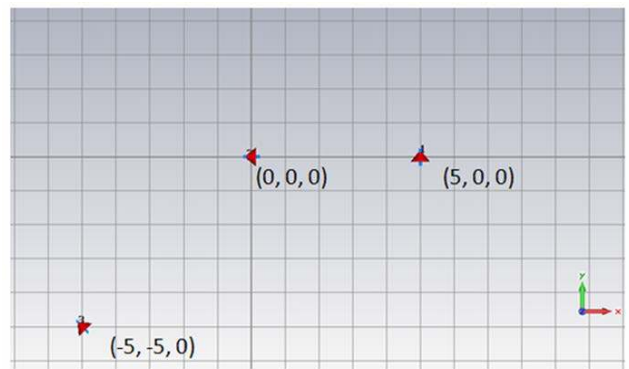


Figure 21: CST MWS simulation setup for the three dipoles from Figure 14.

The results of simulations with CST MWS are displayed in Figures 22.

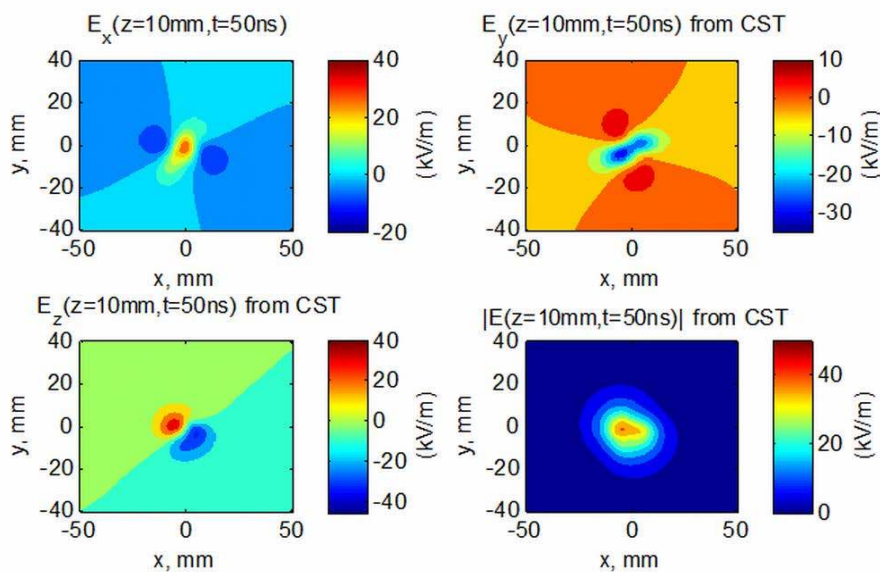


Figure 22: Simulated electric field components E_x , E_y and E_z and the total magnitude $|E|$ for the dipoles in Figure 14 at the horizontal plane at the height $z = 10$ mm at the instant time $t = 50$ ns.

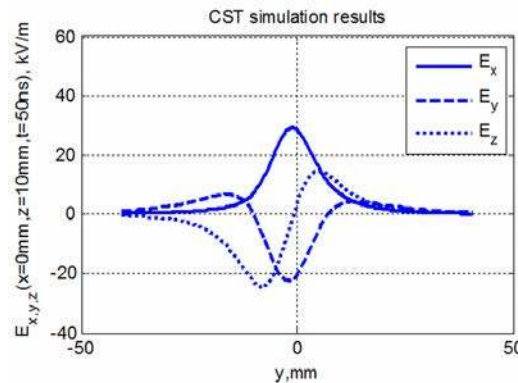


Figure 23: Simulated electric field components E_x , E_y and E_z for the dipoles in Figure 21 along the line $z = 10$ mm and $x = 0$ and at the instant time $t = 50$ ns.

Through these figures, we can see that the simulations and calculation results present a very good correlation. The almost same field distributions are found. However, we can find some differences in the magnitude, when we compare the simulation and calculation results. These differences can be considered as the problem of the mesh sizes of the considered EM simulator.

4. Conclusions

The methodology of time-frequency EM NF computation is successfully developed in this paper. The method proposed consists mainly in convoluting the EM NF obtained from frequency calculation, simulations or measurements in wide frequency band and a steady transient arbitrary waveform perturbations.

In the first part of the paper, theoretical approach illustrating the routine algorithm of the method is established. Then, application by comparing simulations of a microwave device with a standard commercial tool and semi-analytical calculations run in Matlab programming environment was made to verify the validity of the method. To do this, a transient current with pulse waveform presenting some ns time-duration was considered. As expected a good correlation with results from analytical calculation was found.

In the second part of the paper, a transposition of a frequency method based on the PWS spectrum is presented.

The flow chart summarizing the computation of EM wave component X_z from X_x and X_y in 2D is explained. Then, application with the radiation of set of EM dipoles is presented. Once again, as expected a very good correlation with time-domain results from a 3D EM simulation commercial tool is performed.

The approach introduced in this paper can be very useful for time domain EM near field modeling and characterization in EMC application. The methods established is currently extended for the modeling of EM NF emissions based on the set of elementary dipoles [41] based on the frequency models developed in [7-8].

Acknowledgements

Acknowledgement is made to European Union (EU) and Upper Normandy region (FRANCE) for the support of this research through the European INTERREG IVA project No 4081 entitled “Time-Domain Electromagnetic Characterization and Simulation (TECS)”.

References

- [1] T. Yang, Y. Bayram and J. L. Volakis, “Hybrid Analysis of Electromagnetic Interference Effects on Microwave Active Circuits Within Cavity Enclosures,” *IEEE Trans. EMC*, Vol. 52, No. 3, pp. 745-748, Aug. 2010.
- [2] B. Archambeault, C. Brench and S. Connor, “Review of Printed-Circuit-Board Level EMI/EMC Issues and

- Tools,” *IEEE Trans. EMC*, Vol. 52, No. 2, pp. 455-461, May 2010.
- [3] P.-A. Barriere, J.-J. Laurin and Y. Goussard, “Mapping of Equivalent Currents on High-Speed Digital Printed Circuit Boards Based on Near-Field Measurements,” *IEEE Trans. EMC*, Vol. 51, No. 3, pp. 649 - 658, Aug. 2009.
- [4] E. R. Rajkumar, B. Ravelo, M. Bensetti, and P. Fernandez-Lopez, “Application of a hybrid model for the susceptibility of arbitrary shape metallic wires disturbed by EM near-field radiated by electronic structures,” *Progress In Electromagnetics Research (PIER)* B 37, pp. 143-169, 2012.
- [5] E. R. Rajkumar, B. Ravelo, M. Bensetti, Y. Liu, P. Fernandez-Lopez, F. Duval, and M. Kadi, “Experimental Study of a Computational Hybrid Method for the Radiated Coupling Modelling between Electronic Circuits and Electric Cable,” *International Journal of Advanced Engineering Technology (IJAET)*, Vol. 3, No. 1, pp. 1-15, Mar. 2012.
- [6] J. Shi, M. A. Cracraft, J. Zhang and R. E. DuBroff, “Using Near-Field Scanning to Predict Radiated Fields,” *Proc. IEEE Ant. Prop. Int. Symp.*, San Jose, CA, USA, Vol. 3, pp. 1477-1480, 1989.
- [7] Y. Vives-Gilabert, C. Arcambal, A. Louis, F. Daran, P. Eudeline and B. Mazari, “Modeling Magnetic Radiations of Electronic Circuits using Near-Field Scanning Method,” *IEEE Tran. EMC*, Vol. 49, No. 2, pp. 391-400, May 2007.
- [8] Y. Vives-Gilabert, C. Arcambal, A. Louis, P. Eudeline and B. Mazari, “Modeling Magnetic Emissions Combining Image Processing and a Non-Optimization Algorithm,” *IEEE Tran. EMC*, Vol. 51, No. 4, pp. 909-918, Nov. 2009.
- [9] D. Baudry, C. Arcambal, A. Louis, B. Mazari and P. Eudeline, “Applications of the Near-Field Techniques in EMC Investigations,” *IEEE Trans. EMC*, Vol. 49, No. 3, pp. 485-493, Aug. 2007.
- [10] R. Jauregui, M. Pous, M. Fernández and F. Silva “Transient Perturbation Analysis in Digital Radio,” *Proc. IEEE Int. Symp. EMC*, Fort Lauderdale, Florida, USA, pp. 263-268, Jul. 25-30 2010.
- [11] T. Ordas, M. Lisart, E. Sicard, P. Maurine and L. Torres, “Near-Field Mapping System to Scan in Time Domain the Magnetic Emissions of Integrated Circuits,” *Proc. PATMOS’ 08: Int. Workshop on Power and Timing Modeling Optimization and Simulation*, Ver. 1-11, 2009.
- [12] C. E. Baum, “Emerging Technology for Transient and Broad-Band Analysis and Synthesis of Antennas and Scatterers,” *Interaction Note 300, Proc. of IEEE*, pp. 1598-1616, Nov. 1976.
- [13] W. Winter and M. Herbrig, “Time Domain Measurement in Automotive Applications,” *Proc. IEEE Int. Symp. EMC*, Austin, Texas, USA, pp. 109-115, Aug. 17-21 2009.
- [14] R. Cicchetti, “Transient Analysis of Radiated Field from Electric Dipoles and Microstrip Lines,” *IEEE Trans. Ant. Prop.*, Vol. 39, No. 7, pp. 910-918, Jul. 1991.
- [15] S. Braun, E. Gülten, A. Frech and P. Russer, “Automated Measurement of Intermittent Signals using a Time-Domain EMI Measurement System,” *Proc. IEEE Int. Symp. EMC*, Austin, Texas (USA), pp. 232 -235, Aug. 17-21 2009.
- [16] J. Rioult, D. Satharamdoo and M. Heddebaut, “Novel Electromagnetic Field Measuring Instrument with Real-Time Visualization,” *Proc IEEE Int. Symp. EMC*, Austin, Texas (USA), pp. 133-138, Aug. 17-21 2009.
- [17] R. S. Edwards, A. C. Marvin and S. J. Porter, “Uncertainty Analyses in the Finite-Difference Time-Domain Method,” *IEEE Trans. EMC*, Vol. 52, No. 1, pp. 155-163, Feb. 2010.
- [18] L. Liu; X. Cui and L. Qi; “Simulation of Electromagnetic Transients of the Bus Bar in Substation by the Time-Domain Finite-Element Method,” *IEEE Trans. EMC*, Vol. 51, No. 4, Nov. 2009, pp. 1017-1025.
- [19] R. Jauregui, P. I. Riu and F. Silva “Transient FDTD Simulation Validation,” *Proc IEEE Int. Symp. EMC*, Fort Lauderdale, Florida, USA, pp. 257-262, Jul. 25-30 2010.
- [20] M. Adada, “High-Frequency Simulation Technologies-Focused on Specific High-Frequency Design Applications,” *Microwave Engineering Europe*, pp. 16-17, Jun. 2007.
- [21] C. E. Baum, “Some Characteristics of Electric and Magnetic Dipole Antennas for Radiating Transient Pulses,” *Sensor and Simulation Note 405*, Jan. 71.
- [22] B. K. Singaraju and C. E. Baum, “A Simple Technique for Obtaining the Near Fields of Electric Dipole Antennas from Their Far Fields,” *Sensor and Simulation Note 213*, Mar. 76.
- [23] J. Song and K.-M. Chen, “Propagation of EM Pulses Excited by an Electric Dipole in a Conducting Medium,” *IEEE Tran. Ant. Prop.*, Vol. 41, No. 10, pp. 1414-1421, 1993.
- [24] Lakhtakia, V. K. Varadana and V. V. Varadana, “Time-Harmonic and Time-Dependent Radiation by Bifractal Dipole Arrays,” *Int. J. Electronics*, Vol. 63, No. 6, pp. 819-824, Dec. 1987.
- [25] H. G. Schantz, “Electromagnetic Energy around Hertzian Dipoles,” *IEEE Tran. Ant. Prop. Magazine*, Vol. 43, No. 2, pp. 50-62, Apr. 2001.
- [26] W. Jun-Hong, J. L. Lang and J. S. Hui-Sheng, “Optimization of the Dipole Shapes for Maximum Peak Values of the Radiating Pulse,” *Proc. IEEE Tran. Ant. Prop. Society Int. Symp.*, Vol. 1, pp. 526-529, 1997.
- [27] B. Ravelo and Y. Liu, “Computation of Transient Near-Field Radiated by Electronic Devices from Frequency Data”, Chap.1, Fourier Transform Applications, Ed. by Salih Mohammed Salih, Published

- by Intech open science, ISBN 978-953-51-0518-3, Apr. 2012, Rijeka, Croatia, pp. 3-26.
- [28] Agilent E Es of E DA, “Overview: E lectromagnetic Design System (E MDS),” (2 008, S ep.) [O nline]. Available: <http://www.agilent.com/find/eesof-emds>
- [29] ANSYS, “Unparalleled Advancements i n S ignal- and P ower-Integrity, E lectromagnetic Compatibility Testing,” (2009, Jun. 1 6) [Online]. A vailable: <http://investors.ansys.com/>
- [30] North East Systems Associates (NESA), “RJ45 Interconnect Signal Integrity,” (2010 CST Computer Simulation T echnology AG.) [Online]. A vailable: <http://www.cst.com/Content/Applications/Article/Article.aspx?id=243>
- [31] B. Ravelo, Y. Liu, A. Louis and A. K. Jastrzebski, “Study o f hi gh-frequency e lectromagnetic tr ansients radiated by electric dipoles in near-field”, *IET Microw., Antennas Propag.*, Vol. 5, No. 6, pp. 692 - 698, Apr. 2011.
- [32] B. Ravelo, Y . L iu a nd J . B . H . S lama, “ Time-Domain Planar Near-Field/Near-Field Transforms with PWS Method”, *Eur. Phys. J. Appl. Phys. (EPJAP)*, Vol. 53, No. 1, Feb. 2011, 30701-pp. 1-8.
- [33] Y. Liu and B. Ravelo, “On the time-domain near-field radiation with PWS method”, *Proceedings of the Advanced Electromagnetics Symposium (AES) 2012*, Paris, France, Apr. 16-19 2012.
- [34] B. Ravelo, “Electric field Extraction from H-Near-Field in Time-Domain by using PWS Method,” *Progress In Electromagnetics Research (PIER) B*, Vol. 25, 2010, pp. 171-189.
- [35] Y. Liu and B. Ravelo, “Near-field map radiated by structures d isturbed b y a rbitrary tr ansient s ignals”, *Proceedings of the Advanced Electromagnetics Symposium (AES) 2012*, Apr. 16-19 2012, Paris, France.
- [36] C. A . B alanis, *Antenna theory: Analysis and design*, 3rd ed., Wiley, New York, USA, 2005.
- [37] D. T . Paris, W . M . L each a nd E . B . J oy, “Basic theory of probe-compensated near-field measurements,” *IEEE Tran. Ant. Prop.*, Vol. 26, No. 3, pp. 373-379, May 1978.
- [38] J. J. H. Wang, “An examination of the theory and practices of planar near-field measurement,” *IEEE Tran. Ant. Prop.*, 36, vol. 6, pp. 746-753, Jun. 1988.
- [39] J. C. -E. S ten a nd A . H ujanen, “ Aspects o n t he Phase Delay and Phase Velocity in the Electromagnetic Near-Field,” *Progress In Electromagnetics Research (PIER)*, Vol. 56, pp. 67-80, 2006.
- [40] H. R . H ertz, “Untersuchungen u eber d ie Ausbreitung d er E lektrischen K raft,” (in G erman) *Johann Ambrosius Barth*, Leipzig, Germany, 1892.
- [41] Y Liu, B. Ravelo, and P. Fernandez-Lopez, “Modeling of Magnetic Near-Field Radiated by Electronic Devices Disturbed b y Complex T ransient S ignals”, *Applied Physics Research (APR)*, Vol. 4, No. 1, Feb. 2012, pp. 3-18.